Bedload transport in rivers: size matters but so does shape!

Cassel Mathieu*[1], Lavé Jérôme[2], Recking Alain[3], Malavoi Jean-René[5] and Piégay Hervé[1]

[1] University of Lyon, CNRS UMR 5600 Environnement Ville et Société, Site ENS de Lyon, 15 Parvis René Descartes, BP 000F-69342 Lyon Cedex 07, France. casselmathieu@gmail.com and herve.piegay@ens-lyon.fr

[3] CRPG-CNRS, CRPG, Vandœuvre-lès-Nancy, 15, rue Notre Dame des Pauvres BP 20, 54500 Vandœuvre les Nancy, France. jlave@crpg.cnrs-nancy.fr

[4] Inrae, UR ETNA, Domaine Universitaire, 2 rue de la papeterie BP 76, 38402 Saint-Martin-d'Hères, France. alain.recking@inrae.fr

[5] Electricité De France - EDF/DPIH, Département Concessions Eau Environnement Territoires. Le PRIMAT - 190 rue Garibaldi, 69003 LYON, France. jean-rene.malavoi@edf.fr

ABSTRACT

Bedload transport modelling in rivers, which defines the threshold for pebble movement, takes into account the size and density of pebbles, but does not formally consider particle shape. The lack of analyses evaluating the influences of shape and density on particle mobility presents a major deficiency. To address this issue and to compare the relative roles of the density and shape of particles, we performed original sediment transport experiments in an annular flume using molded artificial pebbles equipped with a radio frequency identification tracking system. The particles were designed with four distinct shapes and four different densities while having the same volume, and their speeds and distances traveled under constant hydraulic conditions were analyzed. The results show that particle shape has more influence than particle density on the resting time between particle displacement and the mean traveling distance. For all densities investigated, the particle shape systematically induced differences in travel distance that were strongly correlated ($R^2 = 0.94$) with the Sneed and Folks shape index. Such shape influences,

although often mentioned, are here quantified for the first time, demonstrating why and how they can be included in bedload transport models.

INTRODUCTION

Sediment transport is a key process in fluvial geomorphology, being important for sustainable management of navigable channels, designing engineering projects, predicting morphological changes and associated hydraulic risks, interpreting sedimentary archives and restoring rivers [1]. It involves three phases of particle mobility: (1) entrainment [2–6]; (2) motion [7–9]; and (3) deposition [10,11]. Sediment transport at the particle scale is a stochastic phenomenon [7,12,8,13,14,9], which mostly arises from the complex interactions between particle collisions and highly variable friction, drag, and lift forces due to fluid turbulence. Thus, for practical considerations, empirically calibrated sediment transport functions widely use Shields stress number ($\boldsymbol{\tau^*}$ or $\boldsymbol{\theta}$) to quantify the balance of the forces exerted on the channel bed particles, and the critical Shields number ($\boldsymbol{\tau^*_c}$), which is the threshold value necessary to set particles in motion, to determine the moments at which drag forces exceed stabilizing forces ($\boldsymbol{\tau^*} > \boldsymbol{\tau^*_c}$) and particles can be entrained [15–21]. Such approaches have been used to estimate particle stabilizing forces from median pebble size and submerged density [16]. At the river reach scale, sediment transport estimates generally encapsulate a relation depending on the Shields stress, and therefore also include the median grain size [20,22–27] of the transported sediment.

Published bedload transport datasets from rivers with similar flow conditions, morphologies, and median grain sizes, may show different transport rates, with large variations in the threshold for setting particles in motion [28], variations that can be up to 10-fold [29] around the mean empirical Shields curve [30–32]. To explain such dispersion, many studies have focused on the role of mixed grain size, hiding effects [33–36], macro-roughness, channel steepness, or bed roughness relative to channel depth [37]. However, fewer studies have qualitatively related pebble shape to bedload transport through the influence of pebble angularity [38,39], pebble imbrication [34,35,40], or bed roughness [34,40,41] (i.e. the D/K ratio, where D is the diameter of the particles to be moved and K is the bed-particle diameter). In environments with smooth-beds ($D > K$) and during low to moderate flood events, coarse particles of spherical or ellipsoid shape were observed [42] to be more likely to experience entrainment and transport than flatter shapes. Conversely, in rough-bed rivers ($D < K$), Demir and Walsh[1] found that displacement of flatter shapes (i.e. discs and blades) seems to be promoted. Overall, selective shape entrainment and travel length both decrease as flood magnitude increases and/or particle size decreases [43]. Whereas these previous studies have emphasized that robust deterministic expression of initial motion should encapsulate the role of particle shape and bed roughness in particle motion modelling [38,39,44,45], the scarcity of field and experimental data has prevented a quantitative account of this role.

To partially fill this gap, we designed a parametric study based on experiments run in an annular flume in which the displacements (encapsulating onset motion, travel length and rest periods) of artificial pebbles of various shapes and densities were tracked for several hours. Particle shape has been quantified by many different parametrizations [46–52] expressing angularity, surface roughness, or departure from sphericity. As the latter directly impacts on inertial moments and pivoting angle, we investigated the influence of shape in terms of the departure from sphericity, examining various ellipsoid particle shapes (from plate to blade types).

RESULTS

The number of revolutions made by the monitored particles ranged between 439 laps for an elongated blade and 2270 laps for a sphere, making the lap duration observations were taken from large sample sizes. Although the lap durations within the annular flume displayed large variations (from 3 seconds up to a few minutes; see example in Figure 1) over the total run duration, the cumulative travel distances of the particles (Figure 2) displayed a fairly constant slope that permitted the average traveling velocities of the different artificial pebbles to be defined.

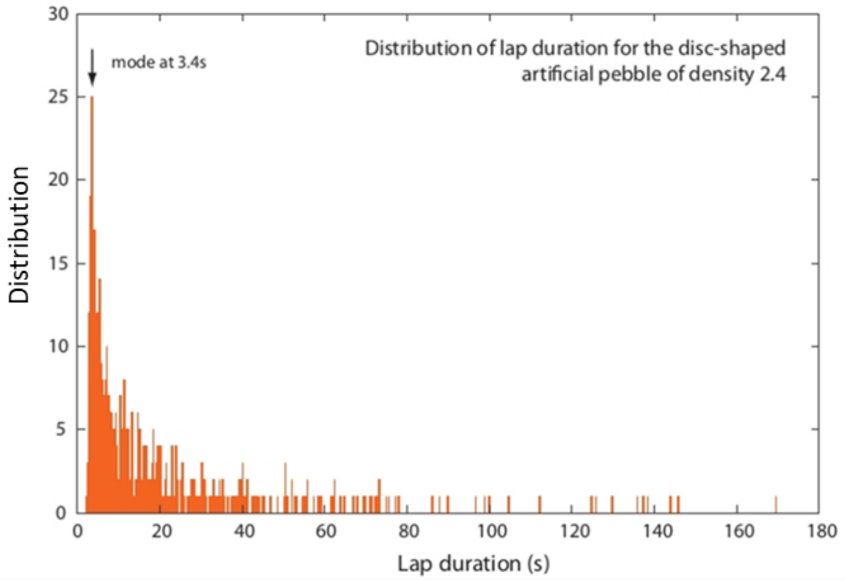

Figure 1. Example of the distribution of lap durations (shape = disc; density = 2.4 g.cm^{-3})

The slight increases observed in the slopes of the cumulative distance curves over time for all shapes and densities reflect the progressive augmentation of the particles' velocities caused by a decrease in the mixing load due to abrasion (relative mass loss of 1.2% per kilometer traveled). As this was moderate and affected all tagged particles in a similar manner, we consider that it had very little impact on the first-order estimates and results of the experiments.

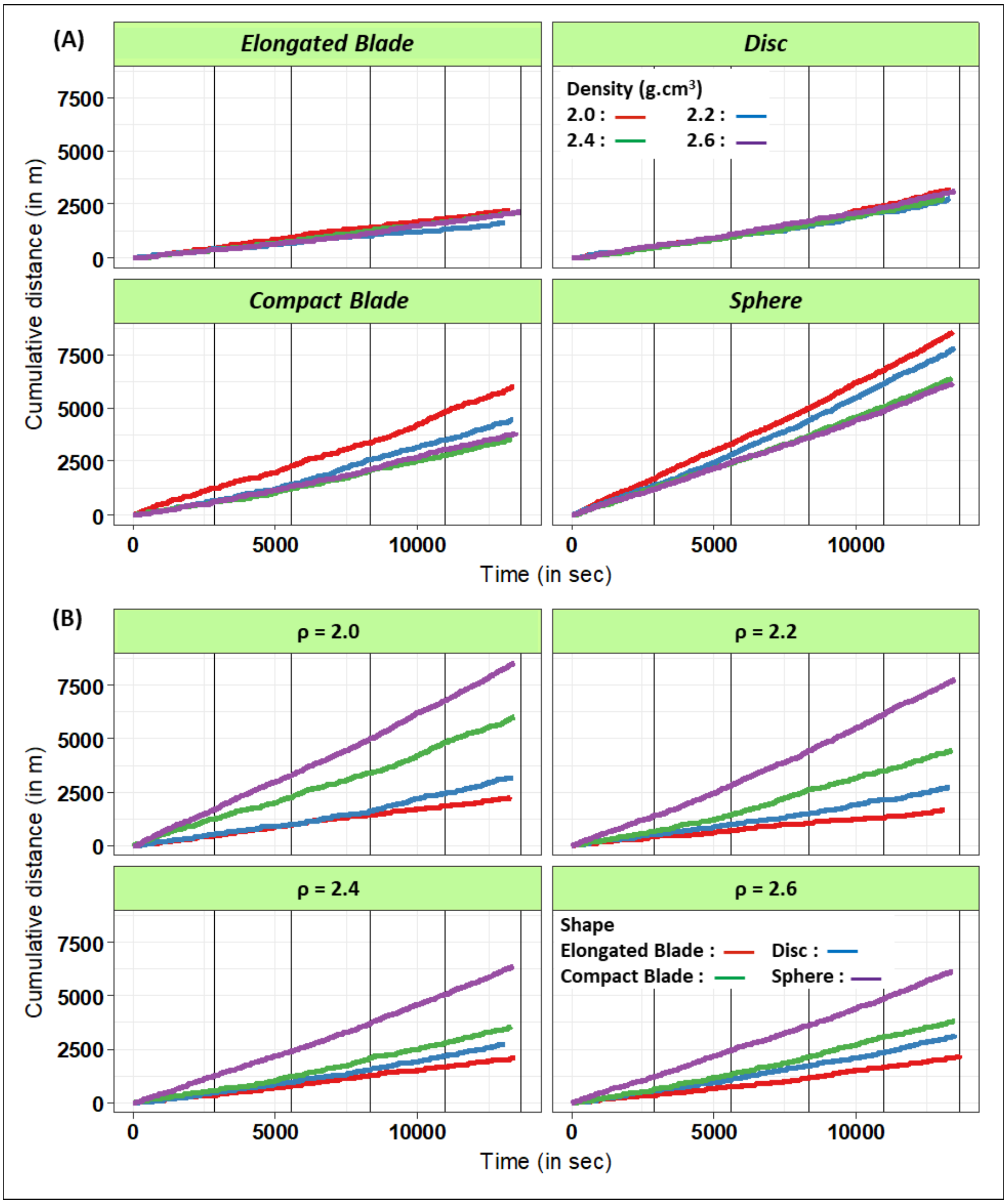

88
89 ***Figure 2. Cumulative travel distances over time according to particle shape (A) and***
90 ***density (B).***

91 The four particle shapes investigated exhibited clear differences in cumulative travel
92 length, with variations in the particle densities also demonstrating effects (Figure 2). The
93 spherical particles traveled the farthest and fastest (mean velocities ranging from 0.44 to 0.60
94 m.s^{-1}), with their mean virtual velocities displaying an inverse relationship with density (Figure
95 3). The compact blade-shaped particles were the second fastest, exhibiting mean velocities
96 ranging from 0.25 to 0.44 m.s^{-1}, again displaying an inverse relationship with density, although

to a lesser extent than that of the spherical particles. In contrast, the mean virtual velocities of the disc- and elongated blade-shaped particles were minimally influenced by their densities: the mean velocities were clustered within a narrow range from 0.14 to 0.17 m.s^{-1}and 0.19 to 0.21 m.s^{-1} respectively. Within the density classes, the distances traveled by the particles clearly showed a high variability in relation to their shapes (Figure 2B and Figure **3**A). The experiments clearly indicate that the variability in velocity associated with pebble shape is substantially higher than that associated with particle density (~100% compared with ~30%).

To explore the influence of particle shape on mobility in a more quantitative way, we used the sphericity index, $\boldsymbol{\Psi_p}$ (1), of Sneed and Folks (1958):

$$\Psi_p = \sqrt[3]{\frac{S^2}{LI}} \qquad \text{Equation (1)}$$

where *L*, *I*, and *S* are the longest, intermediate, and shortest axes of the pebbles.

The sphericity index $\boldsymbol{\Psi_p}$ shows a remarkable positive relationship with the mean traveling velocity (Figure 3B). Moreover, the mean velocities increased from 0.52 to 0.85 m.s^{-1} for decreasing densities from 2.6 to 2.0 g.cm^{-3}. These results suggest that it is possible to estimate differences in the mean virtual velocities and mobilities of particles according to their sphericity.

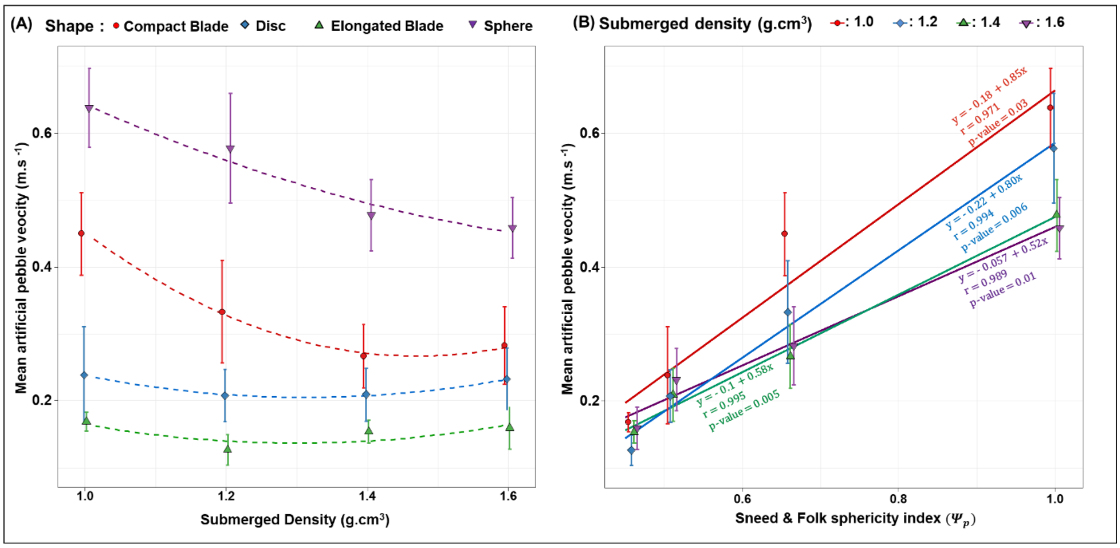

Figure 3. Mean velocity as function of density (A) and Sneed and Folk spherical index (B).

The lap-scaled average travel velocities measured integrate the duration of motion phases and the resting periods in between. However, the pebble shape and density can potentially impact each of these two phases differently. The lap duration distributions are characterized by a first peak at around 3 s in all experiments (Figure 1), which corresponds to a revolution speed of ~1.2 $m.s^{-1}$. For experimental conditions similar to those used in this study, high speed camera viewing[56] previously indicated a mean hop velocity of 1.2 ± 0.2 $m.s^{-1}$ for pebbles in an annular flume. This modal lap duration of ~3 s therefore represents a continuous succession of hops over a full lap, without any resting time. These modal values decrease slightly with increasing density (Figure 4A), as expected from the larger inertial effects after the pebble is set in motion. More importantly, they are almost independent of the pebble shape, as was also observed in a straight flume study[63]. This implies that the impact of shape on the mean traveled distance is mostly caused by its influence on the resting time between movements, i.e. on the immobilization conditions and on the threshold for setting pebbles in motion. To illustrate this inference, a simple calculation of the mean resting time fraction, or immobility ratio (I_r), can be estimated through

$$\mathrm{I}_r = \frac{T - N_l t_m}{T} \quad , \qquad \text{Equation (1)}$$

with T being the total duration of the runs, N_l the number of achieved flume revolutions during T, and t_m the modal lap duration (first mode on the distribution of Figure 1) corresponding to a continuous succession of hops over a full lap.

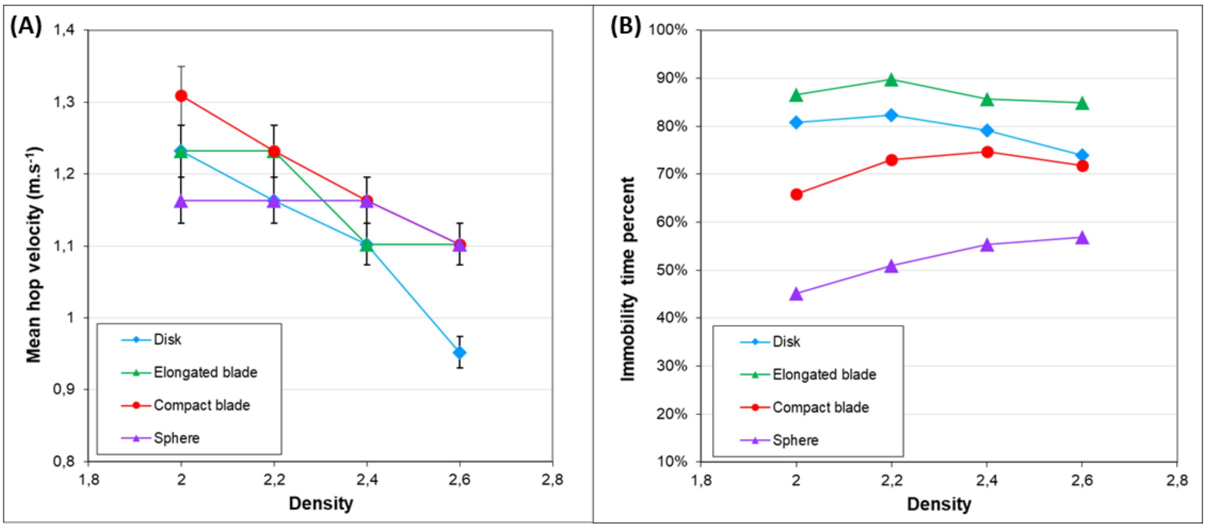

Figure 4. (A) mean hop velocity and (B) time fraction of immobility of the 16 different artificial pebbles.

Except for spherical pebbles that display a slight increase, the immobility ratio (Figure 4B) is only weakly or not affected by the particle density. In contrast, the shape of a pebble deeply impacts its mobility, with the immobility ratio raging from ~50% for the spherical shapes up to ≥85% for the elongated blades.

DISCUSSION

The greater velocity of the spherical and compact-blade-shaped particles relative to the elongated-blade and disc-shaped particles is in good accordance with the literature [1,39,64], given that the flatness of the flume bottom constitutes a low roughness bed surface, despite clustering of temporary resting pebbles. As most lithologies of the pebbles present in rivers show a density close to 2.7 g.cm^{-3}, very similar to the highest value used in this study, we expect their mean velocities to be more strongly influenced by their shape than by their density. On a quantitative basis, this supports the claimed need to include a particle shape parameter in the sediment transport equation [34,41,65].

To do this, we focus on the conditions for setting a particle in motion, because pebble shape has a major influence on virtual velocity through resting periods. Following Komar and

Li's (1986)[41] description, balancing of the moments of tractive and resisting forces for the critical stress yields:

$$\tau_c \propto \frac{l_W \Delta\rho g SIL}{l_D A_a}$$ Equation (2)

where A_a is the apparent section exposed to the flow, and l_D and l_w the respective moment arms of the drag force and submerged weight respectively. Assuming that pebbles tend to lie with their *S*-axis vertically oriented, the moment arms of the drag force l_D approximately scales with the *S*-axis. As a pebble can orient either longitudinally or transversally, we use the intermediate variable $\sqrt{LI}$ to account for the apparent section exposed to the flow ($A_a \propto S\sqrt{LI}$) and the moment arm of the submerged weight l_w. Therefore:

$$\tau_c \cong k\frac{\sqrt{LI}\Delta\rho g\sqrt[3]{(SIL)^2}\widetilde{D}}{S^2\sqrt{LI}} = k\sqrt[3]{\frac{(IL)^2}{S^4}}\Delta\rho g\widetilde{D} = k\frac{1}{\Psi_P^2}\Delta\rho g\widetilde{D}$$ Equation (3)

where k is a function of the particles' Reynold number considered as a constant, $\widetilde{D} = \sqrt[3]{SIL}$, the mean pebble size, and $\Psi_P = \sqrt[3]{\frac{S^2}{IL}}$, the Sneed and Folk's index. Here, $\frac{1}{\Psi_P^2}$ corresponds more or less to the term tan ϕ in Komar and Li (1986): when particle flatness increases (i.e. Ψ_P decreases), the pivoting angle increases and mobility is reduced. Suppressing the unknown k, the threshold can be expressed as:

$$\tau_c \cong \left(\frac{\Delta\rho}{\Delta\rho_{ref}}\right)\left(\frac{\Psi_{\boldsymbol{P_{ref}}}}{\Psi_{\boldsymbol{P}}}\right)^2 \tau_{c_{ref}}$$ Equation (4)

where $\tau_{c_{ref}}$ is the critical Shields stress of a reference pebble of similar size.

The non-dimensional critical threshold is expressed as:

$$\tau_c^* \cong \frac{\tau_c}{\Delta\rho g\widetilde{D}} = \frac{k}{\Psi_P^2} = \left(\frac{\Psi_{\boldsymbol{P_{ref}}}}{\Psi_{\boldsymbol{P}}}\right)^2 \tau^*{}_{c_{ref}}$$ Equation (5)

where $\tau^*{}_{c_{ref}}$ *is* the critical Shields stress of a reference pebble of similar size.

Representing the mean travel velocity of the particle as a function of the critical stress τ_c shows an inverse trend between the two variables (Figure 5): both density and departure from sphericity decrease the ratio of tractive over resistive moments and favor particle immobility.

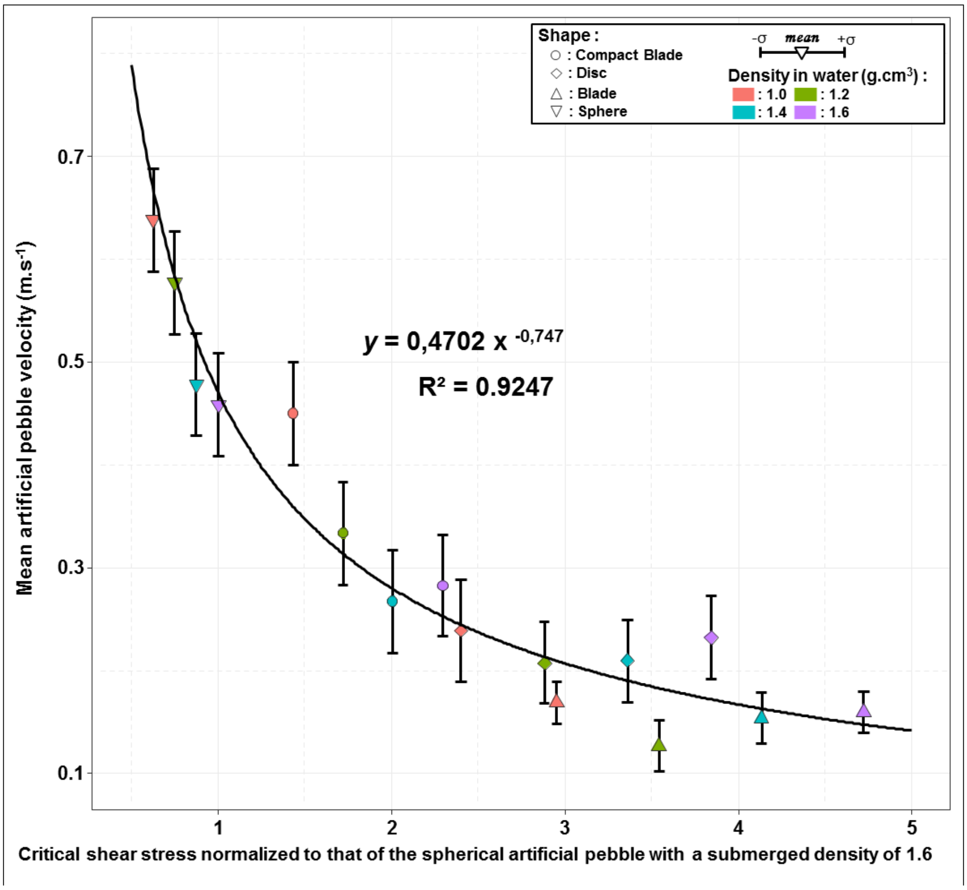

Figure 5. Mean velocity of the 16 artificial pebbles vs. their critical shear stress normalized to that of the spherical artificial pebble with a submerged density of 1.6 (= $\boldsymbol{\frac{\tau_c}{\tau_{c_{ref}}} = \left(\frac{\Delta_\rho}{1.6}\right)\left(\frac{1}{\Psi_P}\right)^2}$***).***

Most bedload transport capacity formulae are functions of the excess Shields stress and follow two general forms: (1) $\Phi = K(\tau^* - \tau_c^*)^\alpha$, and (2) $W^* = (\tau/\tau_c)^\alpha$, where Φ and W^* are two distinct non-dimensional expressions of the bedload transport rate, and α and K two constant terms [66]. To account for the role of pebble shape in a transport capacity relationship, one could introduce into the formula the modified expression for critical shear stress (eq. 4), or the critical Shields stress (eq. 5) that includes the Sneed and Folk Index.

To explore this hypothesis, we built on the fractional transport rate model developed for transport of a mixture of grain sizes (e.g. Parker et al., 1982 [67]). This choice was motivated by the fact that such a relation already proposes a similarity collapse for heterogeneous sediment, which is the case in our experiments with particles of variable shapes and densities mixed with a natural pebble load. We arbitrarily considered Wilcock and Crowe's (2003)[68] relation for fractional transport rate, in which the form of the similarity collapse is:

$$W_i^* = 14\left(1-\frac{0.894}{\phi^{0.5}}\right)^{4.5} \text{ when } \phi = \frac{\tau}{\tau_{ci}} \geq 1.35$$ Equation (6)

where τ is the bed shear stress, τ_{ci} the critical shear stress for incipient motion of a specific pebble *i* (more exactly it corresponds to the minimum shear stress required to achieve a small reference transport rate of $W_i^* = 0.002$ [67]), and W_i^* the dimensionless transport rate $W_i^* = \frac{Rgq_{bi}}{F_i\left(\frac{\tau}{\rho}\right)^{3/2}}$, with $R_i = \frac{\Delta\rho_i}{\rho}$ being the ratio of the submerged sediment (of type *i*) density to water density, g being gravity, q_{bi} the volumetric transport rate per unit width of the particle of type *i* (i.e. of similar shape, size, and density), and F_i the proportion of the pebble type being of the class *i*.

Following our simplified analysis of the force moment balance, we defined the critical (or reference) shear stress as a function (eq. 7) of the mean characteristics of the transported sediment load (i.e. mean gravel size D_m, mean shape factor ψ_{Pm}, and mean density $\Delta\rho_m$) according to:

$$\tau_{ci} = \left(\frac{\Delta_{\rho_i}}{\Delta_{\rho_m}}\right)\left(\frac{\Psi_{Pm}}{\Psi_{Pi}}\right)^2 \tau_{cm}$$ Equation (7)

with τ_{cm} being the critical shear stress for the mean gravel load. Here, $\tau_{cm} = \Delta\rho_m g D_m \tau_c^* \cong 28\,Pa$ considering that $\Delta\rho$ = 2600 kg.m^{-3}, $D_m \approx 5$ cm for the mean gravel diameter of the 65 kg of limestone pebbles, and $\tau_c^* \cong 0.036$ [68].

Within the flume, provided that not all of the particles are in full motion, the conditions of alluvial rivers prevail, i.e. the sediment flux q_{si} is equated by the transport capacity q_{bi}. In our experiments, the mass sediment flux per unit width of the pebble class *i* can be expressed from the mean traveling velocity through: $q_{si} = \frac{F_i M}{\mathrm{A}} V_{gi}$, with A being the surface of the flume bottom, *M* the mass of sediment introduced into the flume, and V_{gi} the mean displacement velocity of particles of type *i*. It follows that a virtual mean velocity can be derived for particle *i* from the above fractional transport rate equation:

$$V_{gi} = \frac{AM\rho_{si}}{R_i g} \left(\frac{\tau}{\rho}\right)^{3/2} W_i^* \left(\frac{\tau}{\tau_{ci}}\right) \qquad \text{Equation (8)}$$

with τ_{ci} derived from equation (7) and a mean shape factor $\Psi_{Pm} = 0.7 \pm -0.08$ for the 65 kg of limestone pebbles.

The virtual velocities derived from the bedload transport relation show a well-defined correlation with the measured virtual velocities (Figure 6). However, the slope of the correlation line is larger than unity, and our modified version of the bedload transport tends to underestimate the observed transport for the densest elongated-blade or disk-shaped pebbles. Despite these slight discrepancies from the observations, these results suggest that the role of pebble shape on bedload transport can be predicted, and that the inclusion of pebble shape characteristics in the modelling of bedload transport offer much promise for improving bedload transport predictions.

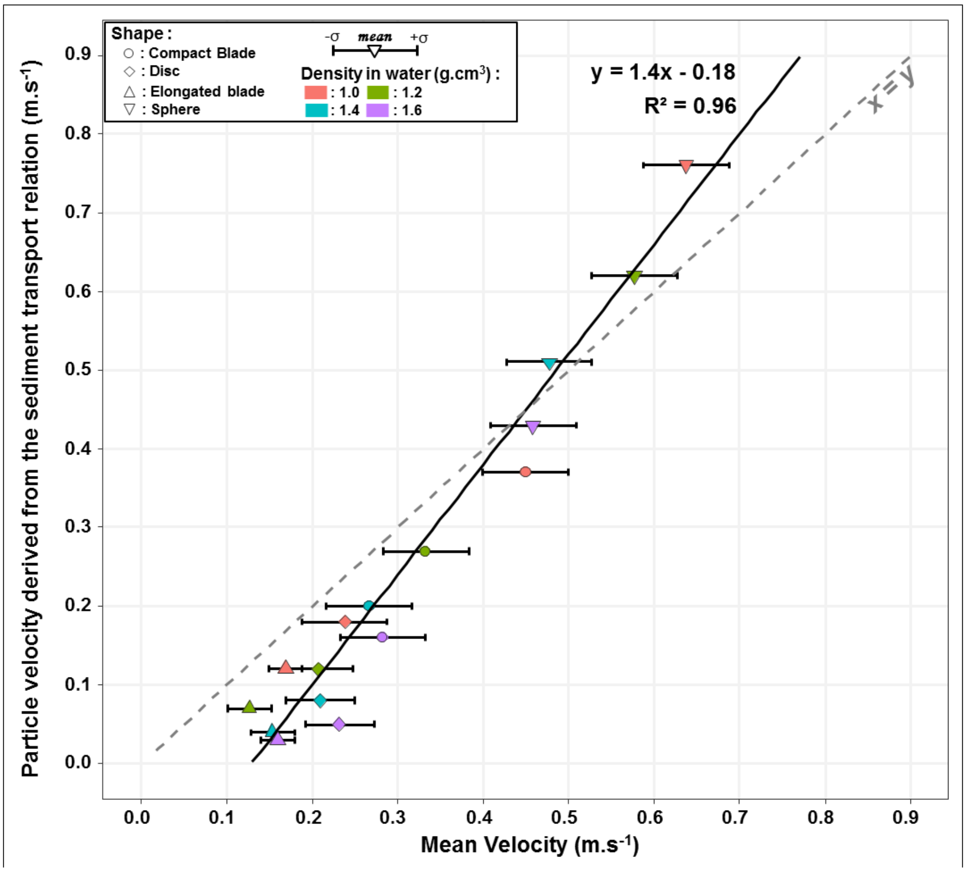

Figure 6. Comparison between the mean measured velocities of particles of various shapes and densities and the theoretical particle velocity derived from a fractional transport rate relation adapted from Wilcock and Crowe's (2003) relation [68].

In terms of sediment dynamics, pebbles travel in the flume following an alternating pattern of resting and motion periods, as generally observed in a natural stream[8]. We therefore consider that our experiments succeeded in capturing the first order behavior of the bedload, and that the introduction of a shape factor into critical Shield stress and bedload transport models might be transposed to rivers. However, the experimental conditions are slightly distinct from those of natural rivers, in particular the use of a monodispersed sediment load and a low-roughness bottom. Additional experiments exploring distinct bottom conditions, grain size distributions, and using straight channels are probably necessary to strengthen our initial results and resolve the slight discrepancies between the model and observations. Similarly, experiments using pebbles with a unique and defined type of particle shape (for example, only platy particles, as expected in sediment derived from the erosion of schist-rich lithologies), instead of a single particle mixed with a large population of pebbles of distinct shapes, should help to derive a more universal relationship. Nevertheless, this study represents a preliminary and promising step towards addressing the role of particle shape in bedload transport.

CONCLUSION

These experiments, based on innovative tools (artificial pebbles of controlled density containing RFIDs) offer new perspectives for studying sediment transport mechanisms. The comparative analysis of the shape and density of particles on their mobility highlights the crucial influence of particle shape. Furthermore, it also indicates that the sphericity index ($\boldsymbol{\Psi_P}$) of Sneed and Folks (1958)[69], which correlates with mean velocity, is relevant for including shape parameters in sediment transport formulae. The method developed in this study can be reproduced to investigate how bed roughness (changing *D/K* ratio) and/or a tracer's grain-size can change the balance between the effects of shape and density on particle velocity. It allows investigation of whether bed roughness promotes the transport of flat-shaped particles, as reported in the literature, and whether particle density can mitigate this effect. Repeating the experiments with smaller particle sizes (maintaining a constant *D/K* ratio) would also allow investigation of whether size mitigates the influence of shape and density on particle transport.

METHODS

We designed four differently-shaped particle models within the grain-size class of 45–64 mm (5.5–6.0 Ψ-units), with all models having the same volume (*i.e.* 49.3 cm^3) but exhibiting differences in the sphericity index [53] (Figure 7A ; Table 1). After creating silicon molds (RTV 120) for these four models, we manufactured 16 artificial pebbles using a mixture of resin and corundum powder in variable proportions, creating pebbles of four different densities (2.0, 2.2, 2.4, and 2.6 g.cm^{-3}) for each mold shape [54]. We equipped these artificial pebbles with transponders of Radio Frequency Identification, RFID, (model RI-TRP-WR2B of Texas Instrument, Dallas Texas USA, also known as PIT Tags) to monitor their displacements within an annular flume[55] (Figure 7B). A detection antenna located on the outside of the flume, along a lateral window, enabled tracking of the number of laps achieved by the RFID-equipped pebbles and the time for each revolution.

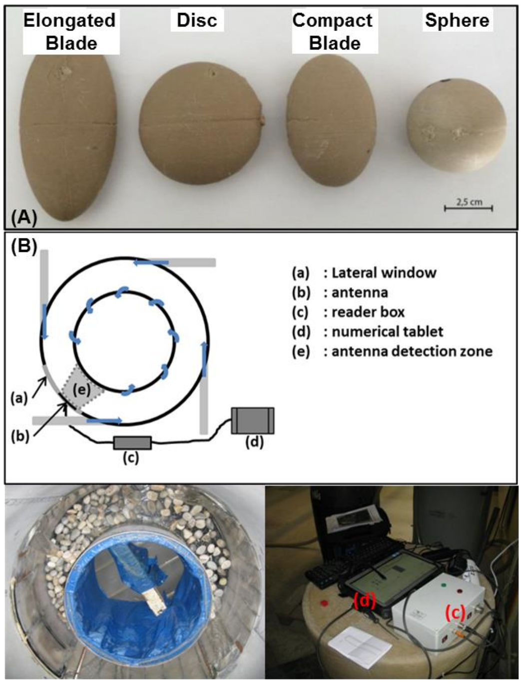

Figure 7. The four particle shapes investigated (A) and the annular flume equipped with the RFID system (B).

Table 1. Shape characteristics of the artificial particles tracked in the flume.

SHAPE	***a*-axis (mm)** *L*	***b*-axis (mm)** *I*	***c*-axis (mm)** *S*	**Vol.(cm^3)**	**Sphericity index (Sneed and Folks, 1958)**
Compact Blade	68.1	46	30	49.3	0.66
Sphere	45.5	45.5	45.5	49.3	1
Disc	65	63	23	49.3	0.51
Elongated Blade	97.2	46.1	21	49.3	0.46

In an attempt to reproduce bedload transport conditions, these artificial pebbles were mixed with 65 kg of limestone pebbles of a similar grain-size (i.e. class 45–64 mm) and were run within an annular flume [56]. A set of experiments were run following the designs of previous studies [54,56,57] for which the sediment dynamics have been characterized[56], i.e. with a low roughness bottom and a monodispersed grain size distribution. During the experiments, the pump discharge sustaining the fluid injection into the flume was maintained at 240 $m^3.h^{-1}$, which for the introduced sediment mass corresponds[56] to a shear stress of $\tau = 135$ Pa at the base of the flume according to Euler theorem applied to the moments, a Shield stress of $\tau^* = 0.16$, a mean transit velocity for pebbles of ≈ 0.4 $m.s^{-1}$, and a sediment flux of ~24 $kg.m^{-1}.s^{-1}$. Under these conditions, high speed camera viewing[56] indicated that the pebbles were transported in the annular flume in a similar manner to that observed[8] in rivers, with alternating transport phases with rolling and saltation, and resting times caused by temporary blockage and piling of particles.

Each experimental run lasted for 45 minutes. To avoid superpositioning of radio-frequency signals and missed RFID transponder detections[54,58,59], only the four particles of the same density were simultaneously present in the flume, thereby also limiting to four the number of transponders. A total of six runs were achieved for the densities of 2.6 and 2.4 $g.cm^{-3}$, and five runs for the densities of 2.0 and 2.2 $g.cm^{-3}$. For each artificial pebble, the combined runs provide a long duration of almost 4 hours and a large cumulative traveled distance, from which the mean traveled velocity (or virtual velocity as defined by Haschenburger and Church[60]) can be computed and the distributions of the lap times estimated. Finally, we compared the virtual velocities and lap distributions of the 16 artificial pebbles, to investigate the effects of the different shapes and densities on bedload transport. In this study, the use of an annular flume enabled the acquisition of a relatively long time series compared with typical straight flume experiments [61] and the sampling of a population of practically uncensored particle trajectories without the limitations induced by a limited detection window or flume length[62]. This ensured that the ranges of traveled distances under conditions of continuous movement were well represented in the experiment. We also made sure that the duration of the experiments (45 minutes) was much longer than the maximum resting time recorded (~5 minutes), to avoid time censorship effects on the distributions of the resting periods and lap times, and to be sure of the statistical significance of the distributions.

References:

1. Demir, T. & Walsh, R. P. D. Shape and size characteristics of bedload transported during winter storm events in the Cwm Treweryn Stream, Brecon Beacons, South Wales. *Turk. J. Earth Sci.* **14**, 105–121 (2005).
2. Mears, A. I. Flooding and sediment transport in a small alpine drainage basin in Colorado. *Geology* **7**, 53 (1979).
3. Bradley, W. C. & Mears, A. I. Calculations of Flows Needed to Transport Coarse Fraction of Boulder Creek Alluvium at Boulder, Colorado. *Geol. Soc. Am. Bull.* **91**, 1057–1090 (1980).
4. Einstein, H. A. & El-Samni, E.-S. A. Hydrodynamic Forces on a Rough Wall. *Rev. Mod. Phys.* **21**, 520–524 (1949).
5. Cheng, E. D. H. & Clyde, C. G. Instantaneous hydrodynamic lift and drag forces on large roughness elements in turbulent open channel flow. in 3-1-3–20 (H. W. Shen, 1972).
6. Komar, P. D. & Li, Z. Applications of grain-pivoting and sliding analyses to selective entrapment of gravel and to flow-competence evaluations. *Sedimentology* **35**, 681–695 (1988).
7. Einstein, H. Bed load transport as a probability problem. 1–105 (1937).
8. Habersack, H. M. Radio-tracking gravel particles in a large braided river in New Zealand: A field test of the stochastic theory of bed load transport proposed by Einstein. *Hydrol. Process.* **15**, 377–391 (2001).
9. Olinde, L. & Johnson, J. Using RFID and accelerometer-embedded tracers to measure probabilities of bed load transport, step lengths, and rest times in a mountain stream. *Water Resour Res* **51**, 7572–7589 (2015).
10. Hjulström, F. Studies of the morphological activity of rivers as illustrated by the River Fyris. Inaugural dissertation,. (Almqvist & Wiksells, 1935).
11. Einstein, A. H. Bedload transport as a probability problem. (Colorado State University, 1937).

12. Ergenzinger, P. & Schmidt, K. H. Stochastic elements of bed load transport in a steppool mountain river. *Hydrol. Mt. Reg. II—Artificial Reserv. Water Slopes Int. Assoc. Hydrol. Sci. Publ.* **194**, 39–46 (1990).
13. Busskamp, R. The influence of channel steps on coarse bed load transport in mountain torrents: case study using the radio tracer technique 'PETSY'. in *Dynamics and geomorphology of mountain rivers* 129–139 (Springer, 1994).
14. Olinde, L. Displacement and entrainment behavior of bedload clasts in mountain streams. (University of Texas, 2015).
15. Shields, A. Application of similarity principles and turbulence research to bed-load movement. *CalTech Libr.* (1936).
16. Meyer-Peter, E. & Müller, R. Formulas for Bed-Load transport. *IAHSR 2nd Meet. Stockh. Append. 2* (1948).
17. Engelund, F. & Hansen, E. A monograph on sediment transport in alluvial streams. *Tech. Univ. Den. 0stervoldgade 10 Cph. K* (1967).
18. Ackers, P. & White, W. R. Sediment Transport: New Approach and Analysis. *J. Hydraul. Div.* **99**, 2041–2060 (1973).
19. Parker, G. & Klingeman, P. C. On why gravel bed streams are paved. *Water Resour. Res.* **18**, 1409–1423 (1982).
20. Recking, A., Frey, P., Paquier, A., Belleudy, P. & Champagne, J. Y. Feedback between bed load transport and flow resistance in gravel and cobble bed rivers: FEEDBACK BETWEEN BED LOAD AND FLOW RESISTANCE. *Water Resour. Res.* **44**, (2008).
21. Piton, G. & Recking, A. The concept of travelling bedload and its consequences for bedload computation in mountain streams: HOW TO ACCOUNT FOR ALLOGENIC SUPPLY IN BEDLOAD TRANSPORT EQUATIONS? *Earth Surf. Process. Landf.* (2017) doi:10.1002/esp.4105.
22. Rickenmann, D. Hyperconcentrated Flow and Sediment Transport at Steep Slopes. *J. Hydraul. Eng.* **117**, 1419–1439 (1991).

23. Smart, G. & Jäggi, M. *Sediment transport on steep slopes. Mitteilung. 64. Versuchsanstalt für Wasserbau, Hydrologie und Glaziologie*. (ETH Zurich, Zurich, 1983).
24. Parker, G., Klingeman, P. C. & McLean, D. G. Bedload and Size Distribution in Paved Gravel-Bed Streams. *J. Hydraul. Div.* **108**, 544–571 (1982).
25. Wilcock, P. R. & Crowe, J. C. Surface-based Transport Model for Mixed-Size Sediment. *J. Hydraul. Eng.* **129**, 120–128 (2003).
26. van Rijn, L. C. Sediment Transport, Part I: Bed Load Transport. *J. Hydraul. Eng.* **110**, 1431–1456 (1984).
27. Recking, A. Theoretical development on the effects of changing flow hydraulics on incipient bed load motion: INCIPIENT MOTION CONDITIONS. *Water Resour. Res.* **45**, (2009).
28. Frey, P. & Church, M. How River Beds Move. *Science* **325**, 1509–1510 (2009).
29. Buffington, J. M. & Montgomery, D. R. A systematic analysis of eight decades of incipient motion studies, with special reference to gravel-bedded rivers. *Water Resour. Res.* **33**, 1993–2029 (1997).
30. Gessler, J. *Chapter 7 Preprint of Paper Beginning and Ceasing of Sediment Motion*. (Colorado State University, 1970).
31. Miller, M. C., McCAVE, I. N. & Komar, P. D. Threshold of sediment motion under unidirectional currents. *Sedimentology* **24**, 507–527 (1977).
32. Yalin, M. S. & Silva, A. M. F. da. *Fluvial processes*. (IAHR, 2001).
33. Miller, R. L. & Byrne, R. J. The angle of repose for a single grain on a fixed rough bed. *Sedimentology* **6**, 303–314 (1966).
34. Li, Z. & Komar, P. D. Laboratory measurements of pivoting angles for applications to selective entrainment of gravel in a current. *Sedimentology* **33**, 413–423 (1986).
35. Kirchner, J. W., Dietrich, W. E., Iseya, F. & Ikeda, H. The variability of critical shear stress, friction angle, and grain protrusion in water-worked sediments. *Sedimentology* **37**, 647–672 (1990).

36. Buffington, J. M., Dietrich, W. E. & Kirchner, J. W. Friction angle measurements on a naturally formed gravel streambed: Implications for critical boundary shear stress. *Water Resour. Res.* **28**, 411–425 (1992).

37. Lamb, M. P., Brun, F. & Fuller, B. M. Hydrodynamics of steep streams with planar coarse-grained beds: Turbulence, flow resistance, and implications for sediment transport: HYDRODYNAMICS OF STEEP STREAMS. *Water Resour. Res.* **53**, 2240–2263 (2017).

38. Miller, R. L. & Byrne, R. J. The Angle of Repose for a Single Grain on a Fixed Rough Bed. *Sedimentology* **6**, 303–314 (1966).

39. Carling, P. A., Kelsey, A. & Glaister, M. S. Effect of bed roughness, particle shape and orientation on initial motion criteria. in *Dynamics of Gravel-bed Rivers* 24–39 (Hey, R.D. Billi, P., Thorne, C.R. and Tacconi, P. (eds), 1992).

40. Lane, E. W. & Carlson, E. J. Some observations on the effect of particle shape on the movement of coarse sediments. *Eos Trans. Am. Geophys. Union* **35**, 453–462 (1954).

41. Komar, P. D. & Li, Z. Pivoting analyses of the selective entrainment of sediments by shape and size with application to gravel threshold. *Sedimentology* **33**, 425–436 (1986).

42. Schmidt, K.-H. & Ergenzinger, P. Bedload entrainment, travel lengths, step lengths, rest periods—studied with passive (iron, magnetic) and active (radio) tracer techniques. *Earth Surf. Process. Landf.* **17**, 147–165 (1992).

43. Schmidt, K.-H. & Gintz, D. Results of Bed load tracer experiments in a mountain river. in *River Geomorphology* 37–54 (Wiley, 1995).

44. Buffington, J. M., Dietrich, W. E. & Kirchner, J. W. Friction angle measurements on a naturally formed gravel streambed: Implications for critical boundary shear stress. *Water Resour. Res.* **28**, 411–425 (1992).

45. White, C. M. The Equilibrium of Grains on the Bed of a Stream. *Proc. R. Soc. Math. Phys. Eng. Sci.* **174**, 322–338 (1940).

46. Zingg, T. Beitrag zur Schotteranalyse. (1935).

47. Barrett, P. J. The shape of rock particles, a critical review. *Sedimentology* **27**, 291–303 (1980).

48. Blott, S. J. & Pye, K. Particle shape: a review and new methods of characterization and classification. *Sedimentology* **55**, 31–63 (2008).

49. Domokos, G., Sipos, A., Szabó, T. & Várkonyi, P. Pebbles, Shapes, and Equilibria. *Math. Geosci.* **42**, 29–47 (2009).

50. Szabó, T. & Domokos, G. A new classification system for pebble and crystal shapes based on static equilibrium points. *Cent. Eur. Geol.* **53**, 1–19 (2010).

51. Domokos, G., Kun, F., Sipos, A. Á. & Szabó, T. Universality of fragment shapes. *Sci. Rep.* **5**, (2015).

52. Novák-Szabó, T. *et al.* Universal characteristics of particle shape evolution by bed-load chipping. *Sci. Adv.* **4**, eaao4946 (2018).

53. Oakey, R. J. *et al.* Grain-Shape Analysis--A New Method for Determining Representative Particle Shapes for Populations of Natural Grains. *J. Sediment. Res.* **75**, 1065–1073 (2005).

54. Cassel, M., Piégay, H. & Lavé, J. Effects of transport and insertion of radio frequency identification (RFID) transponders on resistance and shape of natural and synthetic pebbles: applications for riverine and coastal bedload tracking: Transport and Rfid-Insertion Effects on the Fragility of Pebbles. *Earth Surf. Process. Landf.* (2016) doi:10.1002/esp.3989.

55. Attal, M., Lave, J. & Masson, J. P. New Facility to Study River Abrasion Processes. *J. Hydraul. Eng.* **132**, 624–628 (2006).

56. Attal, M. & Lavé, J. Pebble abrasion during fluvial transport: Experimental results and implications for the evolution of the sediment load along rivers. *J. Geophys. Res.* **114**, (2009).

57. Cassel, M. *et al.* Evaluating a 2D image-based computerized approach for measuring riverine pebble roundness. *Geomorphology* (2018) doi:10.1016/j.geomorph.2018.03.020.

58. Chapuis, M., Bright, C. J., Hufnagel, J. & MacVicar, B. Detection ranges and uncertainty of passive Radio Frequency Identification (RFID) transponders for sediment tracking in gravel rivers and coastal environments. *Earth Surf. Process. Landf.* **39**, 2109–2120 (2014).

59. Arnaud, F., Piégay, H., Vaudor, L., Bultingaire, L. & Fantino, G. Technical specifications of low-frequency radio identification bedload tracking from field experiments: Differences in antennas, tags and operators. *Geomorphology* **238**, 37–46 (2015).

60. Haschenburger, J. K. & Church, M. Bed material transport estimated from the virtual velocity of sediment. *Earth Surf. Process. Landf.* **23**, 791–808 (1998).

61. Cecchetto, M. *et al.* Diffusive Regimes of the Motion of Bed Load Particles in Open Channel Flows at Low Transport Stages. *Water Resour. Res.* **54**, 8674–8691 (2018).

62. Ballio, F., Radice, A., Fathel, S. L. & Furbish, D. J. Experimental Censorship of Bed Load Particle Motions and Bias Correction of the Associated Frequency Distributions. *J. Geophys. Res. Earth Surf.* **124**, 116–136 (2019).

63. Auel, C., Albayrak, I., Sumi, T. & Boes, R. M. Sediment transport in high-speed flows over a fixed bed: 1. Particle dynamics. *Earth Surf. Process. Landf.* **42**, 1365–1383 (2017).

64. Demir, T. The influence of particle shape on bedload transport in coarse-bed river channels. (Durham University, 2000).

65. Bridge, J. S. & Bennett, S. J. A model for the entrainment and transport of sediment grains of mixed sizes, shapes, and densities. *Water Resour. Res.* **28**, 337–363 (1992).

66. Bagnold, R. A. *An approach to the sediment transport problem from general physics*. http://pubs.er.usgs.gov/publication/pp422I (1966).

67. Parker, G., Klingeman, P. C. & McLean, D. G. BEDLOAD AND SIZE DISTRIBUTION IN PAVED GRAVEL-BED STREAMS. *ASCE J Hydraul Div* **108**, 544–571 (1982).

68. Wilcock, P. R. & Crowe, J. C. Surface-based Transport Model for Mixed-Size Sediment. *J. Hydraul. Eng.* **129**, 120–128 (2003).

69. Sneed, E. D. & Folk, R. L. Pebbles in the Lower Colorado River, Texas a Study in Particle Morphogenesis. *J. Geol.* **66**, 114–150 (1958).

Author contributions

M.C., H.P., and J.L. contributed to the design of the experiment. M.C., J.L., and H.P. analyzed experimental results; J.L., H.P., M.C., A.R., and J-R.M. wrote the manuscript.

Corresponding author

Correspondence to Mathieu Cassel.

Competing Interests

The authors declare no competing interests.